ResearchGate

See discussions, stats, and author profiles for this publication at: https://www.researchgate.net/publication/225046801

Active Sites for Outer-Sphere, Inner-Sphere, and Complex Multistage Electrochemical Reactions at Polycrystalline Boron-Doped Diamond Electrodes (pBDD) Revealed with Scanning Electr...

ARTICLE *in* ANALYTICAL CHEMISTRY · MAY 2012

Impact Factor: 5.64 · DOI: 10.1021/ac3010555 · Source: PubMed

CITATIONS
26

READS
209

4 AUTHORS, INCLUDING:

Hollie V Patten
The University of Manchester
13 PUBLICATIONS **95** CITATIONS
SEE PROFILE

Stanley C.S. Lai
University of Twente
31 PUBLICATIONS **1,019** CITATIONS
SEE PROFILE

Julie V Macpherson
The University of Warwick
175 PUBLICATIONS **5,614** CITATIONS
SEE PROFILE

Available from: Julie V Macpherson
Retrieved on: 24 January 2016

analytical chemistry

Article

pubs.acs.org/ac

Active Sites for Outer-Sphere, Inner-Sphere, and Complex Multistage Electrochemical Reactions at Polycrystalline Boron-Doped Diamond Electrodes (pBDD) Revealed with Scanning Electrochemical Cell Microscopy (SECCM)

Hollie V. Patten,[†] Stanley C. S. Lai,[†] Julie V. Macpherson, and Patrick R. Unwin*

Department of Chemistry, University of Warwick, Coventry CV4 7AL, United Kingdom

ABSTRACT: The local rate of heterogeneous electron transfer (HET) at polycrystalline boron-doped diamond (pBDD) electrodes has been visualized at high spatial resolution for various aqueous electrochemical reactions, using scanning electrochemical cell microscopy (SECCM), which is a technique that uses a mobile pipet-based electrochemical cell as an imaging probe. As exemplar systems, three important classes of electrode reactions have been investigated: outer-sphere (one-electron oxidation of ferrocenylmethyltrimethylammonium ($FcTMA^+$)), inner-sphere (one-electron oxidation of Fe^{2+}), and complex processes with coupled electron transfer and chemical reactions (oxidation of serotonin). In all cases, the pattern of reactivity is similar: the entire pBDD surface is electroactive, but there are variations in activity between different crystal facets which correlate directly with differences in the local dopant level, as visualized qualitatively by field-emission scanning electron microscopy (FE-SEM). No evidence was found for enhanced activity at grain boundaries for any of the reactions. The case of serotonin oxidation is particularly interesting, as this process is known to lead to deterioration of the electrodes, because of blocking by reaction products, and therefore cannot be studied with conventional scanning electrochemical probe microscopy (SEPM) techniques. Yet, we have found this system nonproblematic to study, because the meniscus of the scanning pipet is only in contact with the surface investigated for a brief time and any blocking product is left behind as the pipet moves to a new location. Thus, SECCM opens up the possibility of investigating and visualizing much more complex heterogeneous electrode reactions than possible presently with other SEPM techniques.

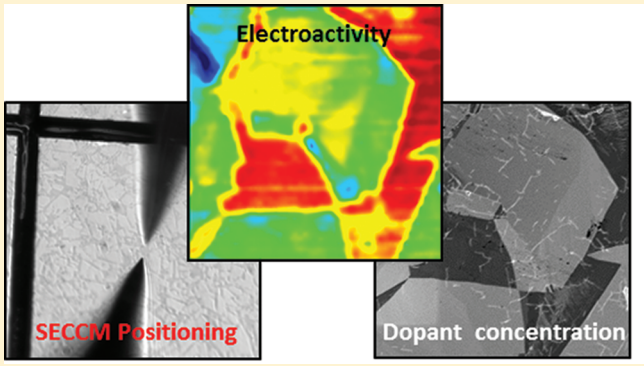

It is now recognized that (i) structural heterogeneities in electrodes have an impact on the rate of local redox reactions, and (ii) a true understanding of electrochemical reactions requires that spatial variations in electroactivity can be visualized.[1] Thus, techniques that identify microscopic activity and relate this to the corresponding properties of the electrode material are highly valued.[2] In this paper, we demonstrate scanning electrochemical cell microscopy (SECCM)[1d,3] as a versatile, high-resolution electrochemical mapping technique, with unique properties that allow it to be used under conditions where other electrochemical imaging techniques would be problematic (for example, where rapid surface film formation and electrode blocking occurs).

The focus of our studies is polycrystalline boron-doped diamond (pBDD), which is a well-known example of a heterogeneous electrode that is finding increasing interest for many applications.[4] We show that SECCM provides unambiguous information on electrode surface reactivity, and that the information obtained is far superior to that obtained with previous electrochemical imaging techniques. Knowledge of how electrochemical reactions proceed on different facets of pBDD is important for the optimization of a wide range of possible applications of this material, from sensing to electrocatalysis.[4] Different crystal faces of pBDD incorporate boron to different extents during growth by chemical vapor deposition. For example, the (111) crystal face may incorporate up to 10 times more boron than the (100) face during synthesis.[5] This heterogeneity in the local concentration of charge carriers, plus other factors such as the possible presence of sp^2 carbon at grain boundaries,[6] has led to speculation in the literature as to whether the entire surface of pBDD is active or whether there are "hot spots" of activity.[6,7] To address possible heterogeneities in electrode reaction rates, various flux imaging techniques have been used, including fluorescence and electrochemiluminescence microscopy[8] and, particularly, scanning electrochemical microscopy (SECM).[6,7] These techniques have highlighted that pBDD electrodes are characterized by spatially heterogeneous electron transfer (HET) rates, but did not have sufficient lateral resolution to resolve individual facets

Received: April 24, 2012
Accepted: May 18, 2012
Published: May 18, 2012

ACS Publications © 2012 American Chemical Society

dx.doi.org/10.1021/ac3010555 | *Anal. Chem.* 2012, 84, 5427−5432

or grain boundaries. Furthermore, a potential drawback of many scanning electrochemical probe microscopy (SEPM) techniques (such as conventional SECM[2e,9]) and SECM with distance control (as in SECM-AFM,[1f,g,10] SECM-SICM,[1h,11] shear force SECM,[12] and intermittent contact (IC)-SECM[1c,13]) is that the sample must be completely immersed in solution. This has three major consequences. First, the spatial resolution depends critically on the electrode size, tip−substrate distance, and the kinetics of the process under investigation. The response of SECM methods is thus complicated (to some extent) by diffusional interactions between different reactive regions on the substrate. Consequently, SECM has proven most powerful in situations where the active sites on substrates are displaced a long distance from each other on an otherwise (largely) inert substrate.[1a,14] Second, imaging with these techniques often requires that the entire electrode substrate is held under conditions where it is active for the time it takes to record an image (which may typically be tens of minutes to hours). Naturally, this can lead to changes in surface properties over time. Finally, in the worst case, extended immersion (and potential control) of the sample may lead to fouling/deactivation of the substrate (during the course of a scan), making SECM-based techniques very challenging for such studies.

These issues are potentially circumvented if the electrochemical imaging technique involves localized contact of solution with the part of the sample investigated for only a short period. This is one of the key attributes of the SECCM technique that we have recently developed,[1d,3] and which greatly extends the capabilities of earlier microdroplet techniques.[15] SECCM enables electrochemical imaging of surfaces via a borosilicate theta pipet as the electrochemical probe. The theta pipet has two barrels, separated by a glass septum, each of which is filled with the redox electrolyte solution of interest and a quasi-reference counter electrode (QRCE). The pipet (and, thus, the electrochemical cell) can either (i) be scanned across the surface, with only the liquid electrolyte droplet at the end of the pipet in contact, to map the surface reactivity, while keeping the tip−substrate separation (i.e., meniscus height) constant, or (ii) be held at a fixed position to perform localized electrochemical experiments such as cyclic voltammetry (CV).

In this paper, we demonstrate the advantages of SECCM in elucidating electrochemical processes at an oxygen-terminated pBDD electrode.[8a,4d,7a] In particular, we demonstrate how the electrochemical activity of individual facets and grain boundaries on pBDD can be determined readily for different classes of electrode reaction and related to the local surface properties. Among the reactions studied is serotonin oxidation during which the electrode is known to foul, making it impossible to study with other electrochemical imaging techniques. Yet, SECCM reveals the heterogeneous activity, and how this relates to the underlying structure, with little impact of the blocking processes.

EXPERIMENTAL SECTION

The SECCM setup has been described recently.[3a,b] In this work, upon approach of the pipet tip to the substrate, a 200 mV bias was applied between the QRCEs, giving rise to a mean conductance current (i_{DC}) across the meniscus formed at the mouth of the pipet, while a small oscillation (ca. 60 nm peak amplitude) was applied to the theta pipet z-position (along the control axis of the pipet, normal to the substrate). When the meniscus comes into contact with a surface, an alternating current component i_{AC} of the conductance current is established, because of the periodic modulation applied to the z-position of the pipet, which modulates the meniscus. An i_{AC} setpoint is used to obtain the maps and to ensure a constant meniscus height, while scanning across the surface.[3b] This was set between 80 pA and 120 pA (∼1% of i_{DC}). The local amperometric current through the pBDD substrate, which is connected as a working electrode, can be measured simultaneously. The substrate is grounded and the potential of the solution adjacent to the substrate is controlled by setting the potential of the two QRCEs (while keeping the potential bias between them fixed); the potential that the substrate experiences is then typically the midpoint of the potential applied to the two QRCEs, but of opposite sign.[3b] In this way the technique provides local functional information on the (electrochemical) properties of the substrate. Tip positioning is aided with an optical system deployed *in situ*, enabling visualization of the tip relative to the substrate.

The pBDD samples were grown using a commercial microwave plasma−chemical vapor deposition (MW-CVD) process (E6 Ltd., Ascot, U.K.). The average boron doping level of this material is $\sim 5 \times 10^{20}$ atoms cm^{-3}, as determined by secondary ion mass spectrometry (SIMS).[7a] The pBDD employed was ca. 500 μm thick and had an average facet size of 5−40 μm. These samples are flat on the scale of SECCM: the roughness is 1−2 nm within a facet and 1−5 nm between grains, as determined by tapping-mode atomic force microscopy (TM-AFM).[4d,16] Before use, samples were acid-cleaned by boiling in concentrated H_2SO_4 (98%), supersaturated with KNO_3, and heated until the KNO_3 had been exhausted.[7a] This treatment results in an oxygen-terminated surface.[17] After acid cleaning, the pBDD sample was rinsed thoroughly with ultrapure water, and electrical contact was made to the back of the sample by sputtering (Moorfield Minibox), first Ti (20 nm), followed by Au (400 nm). The sample was then annealed in a tube furnace (Carbolite, U.K.) at 500 °C for 4 h to create an ohmic titanium carbide contact. The pBDD sample was contacted to a Ti (20 nm)/Au (400 nm) sputter-coated glass slide using silver paint (Agar Scientific, Ltd., U.K.), and electrical contact was made using tinned copper wire contacted to the slide, again using silver paint. To correlate measurements with SECCM and field-emission scanning electron microscopy (FE-SEM) (Zeiss, Model Supra 55-VP) in the same area, the sample was marked with a laser-cut cross with lines ca. 50 μm wide.[7a] This cross, as well as the grain structure of the sample, could be easily visualized using both the optical system on the SECCM and FE-SEM.

SECCM tips were pulled from borosilicate theta capillaries (TG 150-10, Harvard Part No. 30-0114), using a Sutter P-2000 laser puller (Sutter Instruments, USA), and had an inner diameter of ca. 1.5−2.5 μm at the end, determined accurately using FE-SEM. This defines the characteristic spatial resolution of SECCM.[1d,3b] The pulled pipets were filled with a redox active species and supporting electrolyte of interest using a Microfil needle (WPI Instruments) and syringe. All electrochemical measurements are quoted against silver-chloride-coated wire (Ag/AgCl) or Pd−H_2 quasi-reference counter electrodes (vide infra).

All aqueous solutions were prepared from Milli-Q reagent water (Millipore Corp.) with a resistivity of 18.2 MΩ cm at 25 °C. The solutions employed in separate experiments were 2 mM ferrocenylmethyltrimethylammonium ($FcTMA^+$), as the

dx.doi.org/10.1021/ac3010555 | *Anal. Chem.* 2012, 84, 5427−5432

PF_6^- salt prepared in-house from $FcTMA^+I^-$ (Strem Chemicals, Ltd.) via metathesis with $AgPF_6$ (Strem Chemicals, Ltd.) in 50 mM KCl (Sigma–Aldrich); 2 mM iron(II) sulfate ($FeSO_4$) (Sigma–Aldrich) in 0.5 M H_2SO_4 (Sigma–Aldrich); and serotonin (5-hydroxytryptamine; Sigma–Aldrich) in 0.1 M NaCl (Sigma–Aldrich) and 5 mM HEPES (4-(2-hydroxyethyl)-1-piperazineethanesulfonic acid; Fluka), pH 7.

RESULTS AND DISCUSSION

Outer-Sphere Electron Transfer. We first consider a classical outer-sphere redox mediator: the one-electron oxidation of $FcTMA^+$. Figure 1a shows a typical 50 μm × 50 μm SECCM image of the pBDD surface for the oxidation of 2 mM $FcTMA^+$ in 50 mM KCl, using a 1.5-μm diameter pipet. The pBDD substrate was held at a potential (E_{sub}) of 300 mV vs Ag/AgCl, corresponding to an overpotential, η ($E_{sub} - E^{0\prime}$) = −8 mV, where $E^{0\prime}$ is the formal potential. The image was recorded by taking a measurement every 1 μm (itself being the average of 1000 points at a sampling rate of 25 kHz, corresponding to 40 ms per measurement). A corresponding FE-SEM analysis of the same area is shown in Figure 1b, where the lighter and darker areas correspond to less-doped and more-doped facets, respectively, as confirmed by comparison of FE-SEM with other quantitative techniques, as reported previously.[7a] Comparing the electrochemical activity map obtained using SECCM (Figure 1a) with the FE-SEM image (Figure 1b), it is clear that there is a very close correlation between heterogeneities in the HET rate across the surface (as reflected in the SECCM currents) and the underlying facet properties (as shown in the FE-SEM image). In particular, the high spatial resolution of SECCM shows that there are not only differences between grains but also within single facets. Evidently, areas with higher dopant levels yield a higher current, indicative of faster HET kinetics, illustrating that the local dopant level directly impacts the corresponding local electrochemical reactivity for the case of outer-sphere electron transfer (ET). Furthermore, since only a very small area of the surface is in contact with the solution at every imaging point (much smaller than the typical facet size), the SECCM maps unambiguously show that the entire surface of the pBDD is electrochemically active,[7a,b] with no evidence for any increased intrinsic ET rates at grain boundaries, which has previously been proposed as a possible ET mechanism.[6] Interestingly, there was little detectable difference between CVs recorded on the more- and less-doped grains, because changes in the voltammetric wave shape are difficult to detect in the fast kinetic regime.[10b] However, kinetic effects are more readily manifested in changes in the current at constant potential, highlighting another advantage of the imaging approach at constant potential.[3d]

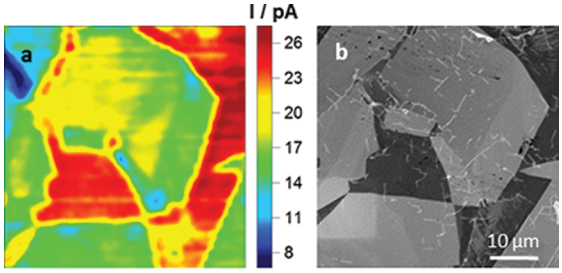

Figure 1. (a) SECCM image (50 μm × 50 μm) showing the oxidation of 2 mM $FcTMA^+$ in 50 mM KCl at 300 mV vs Ag/AgCl (η = −8 mV). (b) Corresponding FE-SEM image of the same area.

Based on the observed current, estimates of the standard HET rate constants (k^0) on the different facet types can be made, based on a meniscus diameter of 1.5 μm in this case, a diffusion coefficient of D_{FcTMA} = 6.0 × 10^{-6} cm^2 s^{-1}, and a transfer coefficient of α = 0.5.[3b] Driving the reaction fully (η = 92 mV) under the same experimental conditions, a mass-transport limiting current of 57 pA was found, corresponding to a mass transport coefficient of ∼0.02 cm s^{-1}. In Figure 1, it can be seen that, at η = −8 mV, the higher-dopant areas display currents of 23.2 ± 1.9 pA (1 σ), which are not significantly different from the theoretical reversible (Nernstian) current (at this potential) of 24.2 pA. Consequently, in the higher-dopant areas, HET is close to reversible under the experimental conditions employed, indicating that k^0 > 0.02 cm s^{-1}. The lower-dopant areas display currents of 16.1 ± 2.0 pA (1 σ), corresponding to an HET rate constant of ∼0.01 cm s^{-1}, determined by finite-element simulations described in detail elsewhere.[3b]

Inner-Sphere Electron Transfer. We turn to the classical inner-sphere redox couple, $Fe^{2+/3+}$.[18] Such HET processes have not been mapped on any electrode surface, to the best of our knowledge. The $Fe^{2+/3+}$ redox couple is generally considered to be sensitive to (the nature of) surface oxygen-containing functional groups on pBDD and carbon electrodes.[18] Because (111) facets are mostly terminated by hydroxyl groups, while the most abundant groups on the (100) facets are ethers or carbonyl groups,[19] this could lead to different interactions of the redox mediator with the surface. Indeed, it has been speculated that the HET kinetics associated with inner-sphere redox couples, such as $Fe^{3+/2+}$, is improved upon oxygen termination of diamond, because of the catalytic effect of the resulting carbonyl groups.[20]

Figure 2a shows a typical 50 μm × 50 μm SECCM activity map for the one-electron oxidation of 2 mM Fe^{2+} in 0.5 M H_2SO_4 (pH ∼ 0.3) at a working electrode potential of 1.2 V (vs Pd–H_2, η = 470 mV) obtained using a ∼1.5-μm-diameter pipet.

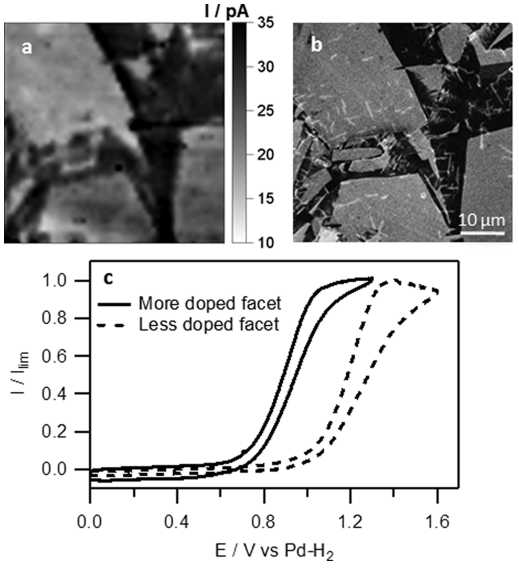

Figure 2. (a) SECCM image (50 μm × 50 μm) of the oxidation of 2 mM Fe^{2+} in 0.5 M H_2SO_4 at 1.2 V vs Pd–H_2 (η = 470 mV). (b) Corresponding FE-SEM image of the same area. (c) CVs recorded on a more- and less-boron-doped facet at a scan rate of 100 mV s^{-1}.

dx.doi.org/10.1021/ac3010555 | Anal. Chem. 2012, 84, 5427–5432

Similar to the outer sphere redox mediator (Figure 1a), the impact of facet structure of the pBDD (see Figures 2a and 2b) on the HET rate is clearly evident in the image, with the more conducting facets again promoting much faster rates of HET. Furthermore, there is again no evidence of enhanced activity at grain boundaries. Note, further, that the difference in electroactivity between the two types of facet is much more distinct than for $FcTMA^{+/2+}$. This difference is especially evident in the CVs recorded by positioning the pipet, with the aid of in situ optical microscopy, on the more- and less-doped facets (see Figure 2c), which show a very clear difference in the onset potential for the oxidation of Fe^{2+} by ca. 300 mV. On the other hand, there is no difference in the quartile potential difference, that is the potential difference of currents at 3/4 and 1/4 of the limiting current value.[21] In both cases, $E_{3/4} - E_{1/4} = 144 \pm 2$ mV (where i_{lim} was taken at a working electrode potential of 1.2 V in the more-conducting region and 1.4 V in the less-conducting region). Such behavior suggests that structural effects of the substrate might be a much more important factor for the reactivity of inner-sphere mediators than for "classical" outer-sphere mediators.

"Complex" Redox Mediator. Finally, we have employed SECCM to study the oxidation of the neurotransmitter serotonin (5-hydroxytryptamine), a "complex" electrochemical reaction involving two electrons and two protons, and complicated further by side reactions.[22] Electrochemistry is widely used as a means of quantitatively measuring serotonin levels in a variety of situations, especially in neurochemistry research, but this is known to be challenging, because serotonin oxidation is notorious for rapidly fouling electrode surfaces upon oxidation.[22] Although pBDD is relatively resistant to electrode fouling during serotonin oxidation, compared to other carbon electrodes,[23] fouling still occurs, especially under conditions of high mass-transport rate. Consequently, conventional electrochemical imaging techniques would be highly problematic for mapping the local reactivity of this process.

We have found that serotonin oxidation rates on pBDD can be imaged successfully to determine local reactivity, even though electrode fouling occurs during SECCM mapping. The advantage of SECCM is that only a tiny fraction of the surface is contacted for a brief period by electrolyte solution during a scan, and the blocking product is left behind in the trail as the pipet probe moves to new locations.

Figure 3a highlights the blocking issue, showing sequential CVs of the oxidation of serotonin (0.5 mM in 5 mM HEPES and 0.1 M NaCl) using a 20 μm × 15 μm theta pipet, covering multiple facets, with a 100 mV s^{-1} scan rate. During potential cycling, fouling of the electrode results in a rapid decrease in the limiting current in each cycle, so that, after 20 cycles, there is essentially no response from the electrode. In contrast, Figure 3b, which was obtained with a ~2.5-μm-diameter pipet, shows a 45 μm × 45 μm SECCM image for the oxidation of 2 mM serotonin in 5 mM HEPES and 0.1 M NaCl (substrate potential held at 0.65 V vs Ag/AgCl, slightly above the experimental half-wave potential). Significantly, a local reactivity map can be recorded with minimal interference from electrode blocking due to the oxidation process. Furthermore, the current magnitude is 179.2 ± 1.1 pA in the high-current regions, which is a value consistent with expectations for a fast (reversible) two-electron process at this potential and with this size pipet.[3b] Moreover, it can again be seen that there is strong correlation between the electrochemical activity map and the corresponding facets in the FE-SEM of the same area, shown in Figure 3c. SECCM provides evidence for a clear difference in HET kinetics for the oxidation of serotonin in the different characteristic facets. Again, the distinctive facet structure of pBDD is reflected in the electrochemical image, and there is no enhanced activity at grain boundaries.

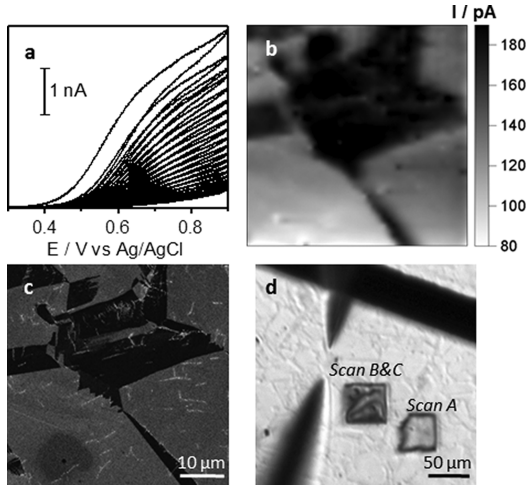

Figure 3. (a) Cyclic voltammograms (CVs) for the oxidation of 2 mM serotonin in 5 mM HEPES and 0.1 M NaCl at a scan rate of 100 mV s^{-1}, using a 20 μm × 15 μm capillary. (b) SECCM image (45 μm × 45 μm) showing the oxidation of 2 mM serotonin at 650 mV vs Ag/AgCl. A clear effect of facet structure is observed. (c) Corresponding FE-SEM image of the same area. (d) SECCM camera image of the pBDD substrate after recording SECCM images. Film formation can be observed after recording one SECCM image (labeled "*Scan A*") and after two images recorded over the same area (labeled "*Scan B & C*"). Also visible is the pipet and its reflection on the surface, the grain structure of the pBDD surface, and a laser-cut line.

The substrate was imaged in situ using the optical microscope of the SECCM positioning system (Figure 3d). This micrograph highlights that during SECCM imaging, serotonin oxidation results in the deposition of an insoluble product on the electrode. Figure 3d shows the film formation after recording one SECCM image ("*Scan A*") and two images at the same location ("*Scan B & C*"). It is evident that there is an increase in film thickness with the number of SECCM scans.

We can attribute the success of SECCM in imaging this challenging electrochemical process to the localized and transient nature of the technique, in which the electrode/electrolyte interface is continuously renewed as the pipet is moved during scanning, leaving behind the product. This demonstrates a major advantage of SECCM over conventional electrochemical imaging methods where the substrate would have been immersed in solution and held under conditions where it would be constantly turning over serotonin, leading to rapid electrode fouling.

■ CONCLUSIONS

The considerable capabilities of scanning electrochemical cell microscopy (SECCM) as a new electrochemical imaging technique have been demonstrated and new information on heterogeneous electron transfer (HET) at polycrystalline boron-doped diamond (pBDD) electrodes has been revealed for outer-sphere, inner-sphere, and complex electrochemical reactions (serotonin oxidation). The main conclusions can be summarized as follows. The entire pBDD surface is electro-

dx.doi.org/10.1021/ac3010555 | *Anal. Chem.* 2012, 84, 5427−5432

chemically active, but apparent HET rates correlate strongly to facet-dependent boron concentration for all three major classes of reaction. Thus, facets with higher boron content have higher HET activity. No evidence of enhanced HET activity at grain boundaries was found for any of the processes. A particularly exciting feature of SECCM is that it can be employed to visualize redox reactions that foul the electrode surface, providing a powerful advantage over conventional scanning electron probe microscopy (SEPM) techniques. The demonstration herein of visualizing serotonin oxidation opens up new possibilities in this arena, particularly of examining complex electrocatalytic reactions on a local scale. In this regard, while SECCM complements SECM-based techniques, it has a clear advantage in the wider range of electrochemical processes that it can address.

AUTHOR INFORMATION

Corresponding Author

*E-mail: p.r.unwin@warwick.ac.uk.

Author Contributions

†These authors contributed equally.

Notes

The authors declare no competing financial interest.

ACKNOWLEDGMENTS

We gratefully acknowledge Dr. Michael Snowden for useful discussions and assistance in data analysis, Mr. Neil Ebejer and Dr. Alex Colburn for assistance with the SECCM instrumentation, and Element Six, Ltd. for providing us with samples. This work was supported by a Marie Curie Intra European Fellowship within FP7 (Project No. 275450 "VISELCAT") to S.C.S.L. and a European Research Council Advanced Investigator Grant (No. ERC-2009-AdG 247143 "QUANTIF") to P.R.U.

REFERENCES

(1) (a) Basame, S. B.; White, H. S. *J. Phys. Chem.* **1995**, *99*, 16430−16435. (b) Basame, S. B.; White, H. S. *Anal. Chem.* **1999**, *71*, 3166−3170. (c) McKelvey, K.; Edwards, M. A.; Unwin, P. R. *Anal. Chem.* **2010**, *82*, 6334−6337. (d) Ebejer, N.; Schnippering, M.; Colburn, A. W.; Edwards, M. A.; Unwin, P. R. *Anal. Chem.* **2010**, *82*, 9141−9145. (e) Shan, X. N.; Patel, U.; Wang, S. P.; Iglesias, R.; Tao, N. J. *Science* **2010**, *327*, 1363−1366. (f) Macpherson, J. V.; Unwin, P. R. *Anal. Chem.* **2000**, *72*, 276−285. (g) Anne, A.; Cambril, E.; Chovin, A.; Demaille, C.; Goyer, C. *ACS Nano* **2009**, *3*, 2927−2940. (h) Takahashi, Y.; Shevchuk, A. I.; Novak, P.; Murakami, Y.; Shiku, H.; Korchev, Y. E.; Matsue, T. *J. Am. Chem. Soc.* **2010**, *132*, 10118−10126. (i) Kim, J.; Xiong, H.; Hofmann, M.; Kong, J.; Amemiya, S. *Anal. Chem.* **2010**, *82*, 1605−1607.

(2) (a) Mirkin, M. V. *Mikrochim. Acta* **1999**, *130*, 127−153. (b) Mirkin, M. V.; Horrocks, B. R. *Anal. Chim. Acta* **2000**, *406*, 119−146. (c) Edwards, M. A.; Martin, S.; Whitworth, A. L.; Macpherson, J. V.; Unwin, P. R. *Physiol. Meas.* **2006**, *27*, R63−R108. (d) Amemiya, S.; Bard, A. J.; Fan, F. R. F.; Mirkin, M. V.; Unwin, P. R. *Annu. Rev. Anal. Chem.* **2008**, *1*, 95−131. (e) Bard, A. J.; Fan, F. R. F.; Kwak, J.; Lev, O. *Anal. Chem.* **1989**, *61*, 132−138. (f) Wittstock, G.; Burchardt, M.; Pust, S. E.; Shen, Y.; Zhao, C. *Angew. Chem., Int. Ed.* **2007**, *46*, 1584−1617. (g) Bard, A. J.; Fan, F. R. F.; Pierce, D. T.; Unwin, P. R.; Wipf, D. O.; Zhou, F. M. *Science* **1991**, *254*, 68−74. (h) Mirkin, M. V.; Nogala, W.; Velmurugan, J.; Wang, Y. *Phys. Chem. Chem. Phys.* **2011**, *13*, 21196−21212. (i) Morris, C. A.; Friedman, A. K.; Baker, L. A. *Analyst* **2010**, *135*, 2190−2202.

(3) (a) Lai, S. C. S.; Dudin, P. V.; Macpherson, J. V.; Unwin, P. R. *J. Am. Chem. Soc.* **2011**, *133*, 10744−10747. (b) Snowden, M. E.; Güell, A. G.; Lai, S. C. S.; McKelvey, K.; Ebejer, N.; O'Connell, M. A.; Colburn, A. W.; Unwin, P. R. *Anal. Chem.* **2012**, *84*, 2483−2491. (c) Lai, S. C. S.; Patel, A. N.; McKelvey, K.; Unwin, P. R. *Angew. Chem., Int. Ed.* **2012**, *52*, 5405−5408. (d) Güell, A. G.; Ebejer, N.; Snowden, M. E.; Macpherson, J. V.; Unwin, P. R. *J. Am. Chem. Soc.* **2012**, *134*, 7258−7261.

(4) (a) Salazar-Banda, G. R.; Eguiluz, K. I. B.; Avaca, L. A. *Electrochem. Commun.* **2007**, *9*, 59−64. (b) Spataru, N.; Zhang, X. T.; Spataru, T.; Tryk, D. A.; Fujishima, A. *J. Electrochem. Soc.* **2008**, *155*, B264−B269. (c) Salazar-Banda, G. R.; Suffredini, H. B.; Avaca, L. A.; Machado, S. A. S. *Mater. Chem. Phys.* **2009**, *117*, 434−442. (d) Hutton, L.; Newton, M. E.; Unwin, P. R.; Macpherson, J. V. *Anal. Chem.* **2009**, *81*, 1023−1032.

(5) (a) Janssen, G.; van Enckevort, W. J. P.; Vollenberg, W.; Giling, L. J. *Diamond Relat. Mater.* **1992**, *1*, 789−800. (b) Samlenski, R.; Haug, C.; Brenn, R.; Wild, C.; Locher, R.; Koidl, P. *Diamond Relat. Mater.* **1996**, *5*, 947−951. (c) Spitsyn, B. V.; Bouilov, L. L.; Derjaguin, B. V. *J. Cryst. Growth* **1981**, *52*, 219−226.

(6) Holt, K. B.; Bard, A. J.; Show, Y.; Swain, G. M. *J. Phys. Chem. B* **2004**, *108*, 15117−15127.

(7) (a) Wilson, N. R.; Clewes, S. L.; Newton, M. E.; Unwin, P. R.; Macpherson, J. V. *J. Phys. Chem. B* **2006**, *110*, 5639−5646. (b) Neufeld, A.; O'Mullane, A. *J. Solid State Electrochem.* **2006**, *10*, 808−816. (c) Wang, S.; Swain, G. M. *J. Phys. Chem. C* **2007**, *111*, 3986−3995.

(8) (a) Colley, A. L.; Williams, C. G.; Johansson, U. D.; Newton, M. E.; Unwin, P. R.; Wilson, N. R.; Macpherson, J. V. *Anal. Chem.* **2006**, *78*, 2539−2548. (b) Chiku, M.; Nakamura, J.; Fujishima, A.; Einaga, Y. *Anal. Chem.* **2008**, *80*, 5783−5787.

(9) (a) Kwak, J.; Bard, A. J. *Anal. Chem.* **1989**, *61*, 1221−1227. (b) Kwak, J.; Bard, A. J. *Anal. Chem.* **1989**, *61*, 1794−1799.

(10) (a) Dobson, P. S.; Weaver, J. M. R.; Holder, M. N.; Unwin, P. R.; Macpherson, J. V. *Anal. Chem.* **2005**, *77*, 424−434. (b) Mirkin, M. V.; Bard, A. J. *Anal. Chem.* **1992**, *64*, 2293−2302. (c) Smirnov, W.; Kriele, A.; Hoffmann, R.; Sillero, E.; Hees, J.; Williams, O. A.; Yang, N.; Kranz, C.; Nebel, C. E. *Anal. Chem.* **2011**, *83*, 4936−4941.

(11) Takahashi, Y.; Shevchuk, A. I.; Novak, P.; Zhang, Y. J.; Ebejer, N.; Macpherson, J. V.; Unwin, P. R.; Pollard, A. J.; Roy, D.; Clifford, C. A.; Shiku, H.; Matsue, T.; Klenerman, D.; Korchev, Y. E. *Angew. Chem., Int. Ed.* **2011**, *50*, 9638−9642.

(12) (a) Ballesteros Katemann, B.; Schulte, A.; Schuhmann, W. *Chem.—Eur. J.* **2003**, *9*, 2025−2033. (b) Hengstenberg, A.; Kranz, C.; Schuhmann, W. *Chem.—Eur. J.* **2000**, *6*, 1547−1554.

(13) McKelvey, K.; Snowden, M. E.; Peruffo, M.; Unwin, P. R. *Anal. Chem.* **2011**, *83*, 6447−6454.

(14) (a) Serebrennikova, I.; White, H. S. *Electrochem. Solid-State Lett.* **2001**, *4*, B4−B6. (b) Ye, H.; Park, H. S.; Bard, A. J. *J. Phys. Chem. C* **2011**, *115*, 12464−12470. (c) Ballesteros Katemann, B.; Schulte, A.; Schuhmann, W. *Electroanalysis* **2004**, *16*, 60−65. (d) Sa, N.; Baker, L. A. *J. Am. Chem. Soc.* **2011**, *133*, 10398−10401. (e) Ishimatsu, R.; Kim, J.; Jing, P.; Striemer, C. C.; Fang, D. Z.; Fauchet, P. M.; McGrath, J. L.; Amemiya, S. *Anal. Chem.* **2010**, *82*, 7127−7134.

(15) (a) Williams, D. E.; Mohiuddin, T. F.; Zhu, Y. Y. *J. Electrochem. Soc.* **1998**, *145*, 2664−2672. (b) Spaine, T. W.; Baur, J. E. *Anal. Chem.* **2001**, *73*, 930−938. (c) Lohrengel, M. M.; Moehring, A.; Pilaski, M. *Fresenius' J. Anal. Chem.* **2000**, *367*, 334−339. (d) Suter, T.; Böhni, H. *Electrochim. Acta* **1997**, *42*, 3275−3280. (e) Suter, T.; Böhni, H. *Electrochim. Acta* **2001**, *47*, 191−199. (f) Williams, C. G.; Edwards, M. A.; Colley, A. L.; Macpherson, J. V.; Unwin, P. R. *Anal. Chem.* **2009**, *81*, 2486−2495.

(16) Hutton, L. A.; Newton, M. E.; Unwin, P. R.; Macpherson, J. V. *Anal. Chem.* **2011**, *83*, 735−745.

(17) (a) Pehrsson, P. E.; Long, J. P.; Marchywka, M. J.; Butler, J. E. *Appl. Phys. Lett.* **1995**, *67*, 3414−3416. (b) Liu, F. B.; Wang, J. D.; Liu, B.; Li, X. M.; Chen, D. R. *Diamond Relat. Mater.* **2007**, *16*, 454−460.

(18) Chen, P.; McCreery, R. L. *Anal. Chem.* **1996**, *68*, 3958−3965.

(19) (a) Thomas, R. E.; Rudder, R. A.; Markunas, R. J. *J. Vac. Sci. Technol., A* **1992**, *10*, 2451−2457. (b) Nebel, C. E.; Ristein, J. *Thin-Film Diamond II*; Elsevier Academic Press: Amsterdam, 2004.

(20) Fischer, A. E.; Show, Y.; Swain, G. M. *Anal. Chem.* **2004**, *76*, 2553−2560.

(21) Bard, A. J.; Faulkner, L. R. *Electrochemical Methods: Fundamentals and Applications*, 2nd Edition; Wiley: New York, 2001.
(22) (a) Sarada, B. V.; Rao, T. N.; Tryk, D. A.; Fujishima, A. *Anal. Chem.* **2000**, *72*, 1632−1638. (b) Wrona, M. Z.; Dryhurst, G. *J. Org. Chem.* **1987**, *52*, 2817−2825. (c) Wrona, M. Z.; Dryhurst, G. *J. Electroanal. Chem. Interfacial Electrochem.* **1990**, *278*, 249−267.
(23) Güell, A. G.; Meadows, K. E.; Unwin, P. R.; Macpherson, J. V. *Phys. Chem. Chem. Phys.* **2010**, *12*, 10108−10114.